Journal of Power Sources 270 (2014) 21–27

Contents lists available at ScienceDirect

Journal of Power Sources

journal homepage: www.elsevier.com/locate/jpowsour

The microstructures and electrochemical performances of $La_{0.6}Gd_{0.2}Mg_{0.2}Ni_{3.0}Co_{0.5-x}Al_x$ (x=0–0.5) hydrogen storage alloys as negative electrodes for nickel/metal hydride secondary batteries

Rongfeng Li, Peizhen Xu, Yamin Zhao, Jing Wan, Xiaofang Liu, Ronghai Yu*

School of Materials Science and Engineering, Beihang University, Beijing 100191, China

HIGHLIGHTS

- The substitution Al for Co for A_2B_7-type alloy electrodes was scarcely reported.
- The cooperation of Al and Co yield alloys with superior electrochemical performances.
- The mechanism of capacity degradation for alloy electrodes after Al substitution was provided.

ARTICLE INFO

Article history:
Received 17 May 2014
Received in revised form
14 July 2014
Accepted 15 July 2014
Available online 22 July 2014

Keywords:
Hydrogen storage alloy
Element substitution
Cyclic stability
Electrochemical kinetics

ABSTRACT

$La_{0.6}Gd_{0.2}Mg_{0.2}Ni_{3.0}Co_{0.5-x}Al_x$ (x = 0–0.5) hydrogen storage alloys were prepared by induction melting followed by annealing treatment at 1173 K for 8 h. The effects of substitution Al for Co on the microstructures and electrochemical performances were studied systematically. The structure analyses show that all alloys consist of multiphase structures such as $(La, Mg)_2Ni_7$ phase, (La, Mg) Ni_3 phase and $LaNi_5$ phase. The abundance of $(La, Mg)_2Ni_7$ phase decreases while the abundance of $LaNi_5$ phase and (La, Mg) Ni_3 phase increases directly as the Al content increasing. The electrochemical tests show that the maximum discharge capacity of alloy electrodes are almost unchanged when $x \leq 0.2$ while the cyclic stability of the alloy electrode are improved significantly after proper amount of Al substitution for Co. The alloy electrode with $x = 0.1$ exhibits the better balance between discharge capacity and cycling life than any others. Moreover, at the discharge current density of 900 mA g^{-1}, the high rate dischargeability (HRD) of the alloy electrodes decreases with increasing Al substitution and the relative analyses reveal that the charge transfer on alloy surface is more important than the hydrogen diffusion in alloy bulk for the kinetic properties of the alloy electrodes.

1. Introduction

Because of many advantages such as high energy density, perfect activation properties and environmentally friendliness, Ni/MH batteries have been occupying a large market share in secondary battery filed. As negative electrode material of Ni/MH batteries, the conventional rare earth-based AB_5-type hydrogen storage alloys which have been commercialized suffer from low discharge capacity (320 mAh g^{-1}) due to its $CaCu_5$-type crystal structure. The newly La–Mg–Ni system hydrogen storage alloys such as A_2B_7-type and AB_3-type alloys are considered to be the most promising candidates to replace AB_5-type alloys because of the higher discharge capacity (400 mAh/g) [1–3]. However, it is necessary to improve the cyclic durability of this kind of alloy in the alkaline electrolyte for the practical application. Element substitution has been proved to be an effective way to improve the overall electrochemical properties of hydrogen storage alloys. Among the substitution elements, Co is thought to play an important role to improve the cycle life of La–Mg–Ni system hydrogen storage alloys because it can increase the corrosion resistance of the electrodes in the alkaline electrolyte [4,5]. Notten [6] confirmed that Co addition can effectively improve cycle life of MH/Ni secondary batteries. Liu [7] reported that the cycling stability of $La_{0.7}Mg_{0.3}Ni_{3.4-x}Mn_{0.1}Co_x$ (x = 0–1.3) alloy electrodes was markedly improved from 25.5% (x = 0) to 61.3% (x = 1.3) after 90 cycles because of the lower oxidation/corrosion rate with Co addition. Actually, the effects of Co substitution for Ni on electrochemical properties of La–Mg–Ni

* Corresponding author. Tel.: +86 10 82313786.
E-mail addresses: luckylrf@163.com (R. Li), rhyu@buaa.edu.cn, rhybuaa@163.com (R. Yu).

http://dx.doi.org/10.1016/j.jpowsour.2014.07.092
0378-7753/

system hydrogen storage alloys have been studied extensively. However, the cycle life of this kind of alloy still not meets the demands of the market by simply Co substitution. Moreover, Co is the most expensive element in such alloys which resists the further commercial application. Consequently, for La–Mg–Ni system alloys, it is important to find an effective way to improve the cycle life further and decrease Co content. Al is another key substitution element to improve the cyclic stability of hydrogen storage alloys which is much more cheaper than Co. Partially substituting Ni with Al can prolong the cycling life of the hydrogen storage alloy electrodes because of forming a dense oxide film which can prevent alloys from further corrosion in KOH electrolyte, however, the discharge capacity of the alloy electrodes decreases too much after Al substitution [8–10]. Dong [11] revealed that Al substitution could prolong the cyclic lifetime of the La–Mg–Ni system alloy electrodes from 55.45% to 70.08% after 100 cycles while the maximum discharge capacity decreased from 401.8 mAh/g to 373.7 mAh/g. Liao [12] found that the cycling stability of the La–Mg–Ni system alloy electrodes could be improved further by Al substitution than by some other elements such as Co, Cu, Fe, Mn and Sn while the alloy electrode with Al substitution showed the minimum discharge capacity which was only 185.4 mAh/g. Based on the effects of Al and Co substitution for Ni on the electrochemical properties for La–Mg–Ni-system hydrogen storage alloys respectively, it is expected that the combination of Al and Co which are used as a group of substitution elements may yield alloys with superior electrochemical performances. As a result, it is essential and important to study the correlations of Co and Al on microstructures and electrochemical performances of La–Mg–Ni system alloys for the further commercial applications.

In our previous research, we found that the addition of Gd with proper content can improve the overall electrochemical properties of the alloy electrodes effectively and the alloy with chemical composition of $La_{0.6}Gd_{0.2}Mg_{0.2}Ni_{3.0}Co_{0.5}$ possesses good electrochemical performances such as discharge capacity and cyclic stability. So in this paper, $La_{0.6}Gd_{0.2}Mg_{0.2}Ni_{3.0}Co_{0.5-x}Al_x$ ($x = 0$–0.5) alloys were prepared and the effects of substituting Al for Co on microstructures and electrochemical properties were investigated systematically.

2. Experimental

$La_{0.6}Gd_{0.2}Mg_{0.2}Ni_{3.0}Co_{0.5-x}Al_x$ ($x = 0$–0.5) hydrogen storage alloys were prepared by vacuum induction melting on a water-cooled cooper crucible under 0.2 MPa argon atmosphere followed by annealing treatment at 1173 K for 8 h. Due to the high vapor pressure of Mg element, an appropriate excess (10 wt.%) of Mg element was necessary. The purity of all elements was above 99.9 wt.%.

The annealed alloys were mechanically crushed and ground into powders of 400 mesh size for X-ray diffraction (XRD) measurements and into powders of 300–400 mesh size for electrode test. The crystal structures were determined by XRD analyses which were carried out by a Rigaku D/max-2500 diffractometer. The diffraction was performed with Cu Kα1 radiation filtered by graphite. The experimental parameters were 40 kV, 200 mA, and 4° min^{-1}. Then the collected data were analyzed by the Rietveld method using Fullprof 2K software to get the lattice parameters and phase abundance.

All the test electrodes were prepared by cold pressing the mixture of 0.1 g alloy powder and 0.3 g carbonyl nickel powder under 15 MPa pressure to form a pellet of 10 mm in diameter. The additive carbonyl nickel powder was used to increase the electrocatalytic activity and decrease the electrochemical reaction resistance of the alloy electrodes. Then the pellet was sandwiched within two foamed Ni plates with a Ni wire soldered on to form a negative electrode. The electrodes were immersed in 6 M KOH solution for 6 h in order to wet thoroughly before electrochemical measurements. Electrochemical measurements were performed at 298 K in a standard open tri-electrode electrolysis cell consisting of a working electrode (the MH electrode for studying), a sintered $Ni(OH)_2$/NiOOH counter electrode with excess capacity and a Hg/HgO reference electrode, immersed in the electrolyte of 6 M KOH solution. For activation, each electrode was charged at 60 mA g^{-1} for 7.5 h followed by a 10 min rest and then discharged at 60 mA g^{-1} to the cut off potential of −0.6 V (vs. Hg/HgO reference electrode). For cycling test, the activated electrode was charged at 100 mA g^{-1} for 4.5 h followed by a 10 min rest and then discharged at 300 mA g^{-1} to the cut off potential of −0.6 V (vs. Hg/HgO reference electrode). The high rate dischargeablity (HRD) of the alloy electrodes was determined by examining the discharge capacity at various discharge current densities and defined as the following equation:

$$HRD_i = \frac{C_i}{C_i + C_{100}} \times 100\% \quad (1)$$

where C_i is the discharge capacity with a cut-off potential of −0.6 V (vs. Hg/HgO reference electrode) at i current density, C_{100} is the residual discharge capacity to the same cut-off potential at current density i = 100 mA g^{-1} after the alloy electrode is discharged at current density i. The data were collected in an automatic Arbin MSTAT battery testing instrument.

To investigate the mechanism of discharge capacity degradation and the kinetics character of alloy electrodes, linear polarization, Tafel polarization, and potential-step discharge method were performed on Princeton VersaSTAT MC electrochemical work station after alloy electrodes were fully activated. The linear polarization curves and the Tafel polarization curves were measured by scanning the electrode potential at a rate of 0.1 mV s^{-1} from −5 to 5 mV (vs. open circuit potential) and 5 mV s^{-1} from −1.2 V to −0.2 V (vs. Hg/HgO reference electrode), respectively, at 50% depth of discharge (DOD). The hydrogen diffusion coefficient was estimated by the potential-step discharge method. The experiment was carried out on Princeton VersaSTAT MC electrochemical work station. The full-charged electrodes were discharged at an overpotential of +600 mV for 4000 s. In addition, the microstructure evolution of the alloy particles after certain charge/discharge cycles was observed by scanning electron microscope (SEM) on a CS3400 instrument.

3. Results and discussion

3.1. Crystal structures

Fig. 1 shows the XRD patterns of $La_{0.6}Gd_{0.2}Mg_{0.2}Ni_{3.0}Co_{0.5-x}Al_x$ ($x = 0$–0.5) hydrogen storage alloys. As shown in Fig. 1, the phase structures of the alloys were changed with Al substitution for Co. Fig. 2 illustrates the example of XRD pattern and Rietveld analysis pattern of the $La_{0.6}Gd_{0.2}Mg_{0.2}Ni_{3.0}Co_{0.4}Al_{0.1}$ alloy. Fig. 3 shows the phase structure of the alloys. Phase abundance, lattice parameters and unit cell volumes are listed in Table 1, which were calculated from the data of Fig. 1 with Rietveld method. As seen from Fig. 1 and Table 1, all alloys have multiphase structures including $(La, Mg)_2Ni_7$ phase, (La, Mg) Ni_3 phase and $LaNi_5$ phase. From Table 1 and Fig. 3, it can be found that as Al content increasing, the abundance of $(La, Mg)_2Ni_7$ phase decreases from 91.09% ($x = 0$) to 89.31% ($x = 0.1$) slightly and then decreases to 37.98% ($x = 0.5$) while the abundances of $LaNi_5$ phase and $(La, Mg)Ni_3$ phase increase directly from 3.11% ($x = 0$) to 46.76% ($x = 0.5$) and from 5.80% ($x = 0$) to 15.26% ($x = 0.5$), respectively. The results of structure analyses show that Al

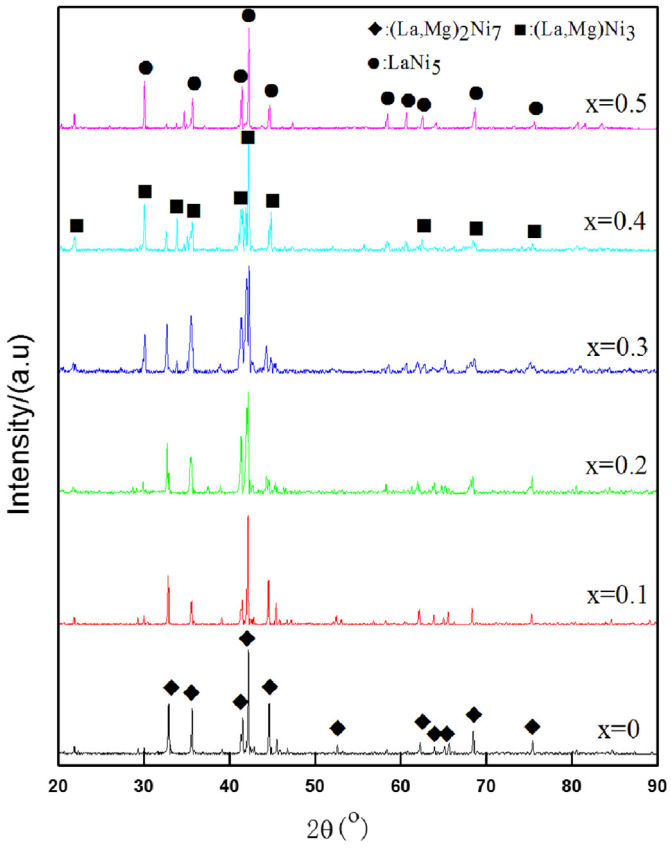

Fig. 1. XRD patterns of $La_{0.6}Gd_{0.2}Mg_{0.2}Ni_{3.0}Co_{0.5-x}Al_x$ ($x = 0$–0.5) alloys.

addition causes the transformation of (La, Mg)$_2$Ni$_7$, (La, Mg)Ni$_3$ and LaNi$_5$ phases. When the amount of Al increases, the structure of (La, Mg)$_2$Ni$_7$ phase become unstable and decompose into (La, Mg)Ni$_3$ and LaNi$_5$ phases which is the same trend as previous research [13]. In addition, the unit cell volumes of various phases increase linearly with increasing x, which is mainly attributed to the atomic radius of Al (1.82 Å) is larger than that of Co (1.67 Å).

3.2. Activation performance and discharge capacity

Fig. 4 shows the activation curves of $La_{0.6}Gd_{0.2}Mg_{0.2}Ni_{3.0}Co_{0.5-x}Al_x$ ($x = 0$–0.5) alloy electrodes. Electrochemical

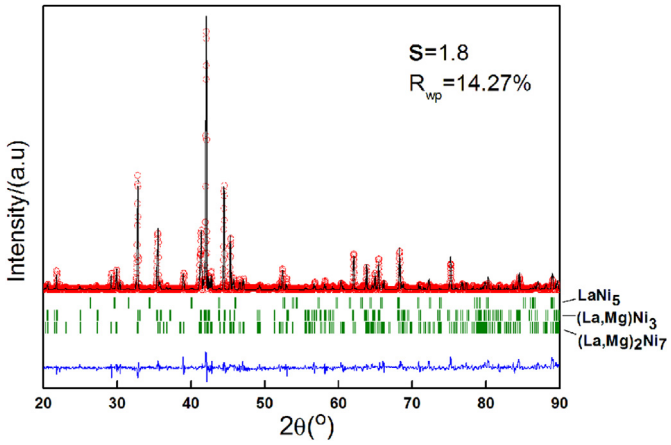

Fig. 2. Example of XRD pattern and Rietveld analysis pattern of $La_{0.6}Gd_{0.2}Mg_{0.2}Ni_{3.0}Co_{0.4}Al_{0.1}$ alloy.

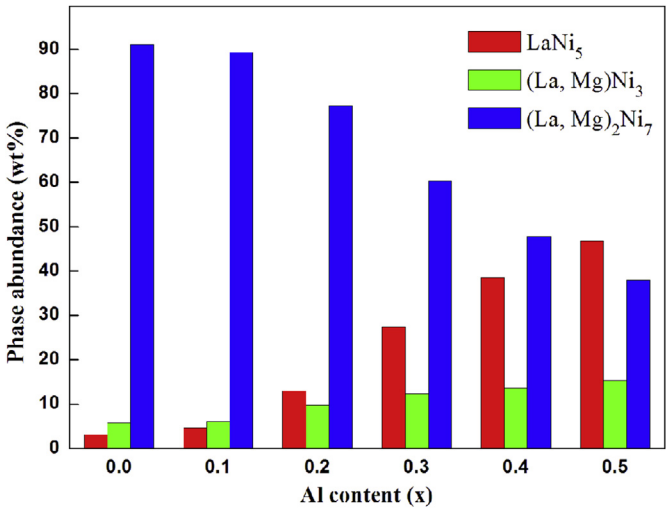

Fig. 3. Phase structure of $La_{0.6}Gd_{0.2}Mg_{0.2}Ni_{3.0}Co_{0.5-x}Al_x$ ($x = 0$–0.5) alloys.

characteristics of the alloy electrodes are summarized in Table 2. The results show that all alloy electrodes possess excellent activation capability and can be fully activated within three cycles which would make them attractive in practical applications. Meanwhile, it can be seen that Al substitution for Co can evidently influence the discharge capacity of alloy electrodes. The maximum discharge capacity of the alloy electrodes is about 390 mAh/g when $x \leq 0.1$, when $x \geq 0.2$, the discharge capacity decreases from 384.3 mAh/g ($x = 0.2$) to 308.4 mAh/g ($x = 0.5$) gradually with increasing Al content. According to the phase structure analysis, it can be found that as the Al content increasing, the abundance of (La, Mg)$_2$Ni$_7$ phase decreases while that of LaNi$_5$ phase increases remarkably. It is known that the discharge capacity of alloy electrodes with (La, Mg)$_2$Ni$_7$ phase is lager than that of the LaNi$_5$ phase [14,15]. Hence, the decreasing discharge capacity with Al substitution can be mainly attributed to the transformation of the phase abundance in alloys.

3.3. Cyclic stability

The cycling life of the La–Mg–Ni system hydrogen storage alloy electrodes is the key problem for their practical applications. Fig. 5

Table 1
Characteristics of phases in $La_{0.6}Gd_{0.2}Mg_{0.2}Ni_{3.0}Co_{0.5-x}Al_x$ ($x = 0$–0.5) alloys.

x	Phase type	Phase abundance (wt%)	Lattice constant (Å)		Cell volume (Å^3)
			a	c	
0	LaNi$_5$	3.11	5.027	3.979	87.08
	(La, Mg)Ni$_3$	5.80	4.969	24.878	531.95
	(La, Mg)$_2$Ni$_7$	91.09	5.039	24.286	534.04
0.1	LaNi$_5$	4.63	5.032	3.988	87.45
	(La, Mg)Ni$_3$	6.06	4.985	24.885	535.53
	(La, Mg)$_2$Ni$_7$	89.31	5.044	24.321	535.87
0.2	LaNi$_5$	12.99	5.036	4.014	88.16
	(La, Mg)Ni$_3$	9.69	5.046	24.345	536.81
	(La, Mg)$_2$Ni$_7$	77.32	5.053	24.386	539.23
0.3	LaNi$_5$	27.45	5.043	4.026	88.67
	(La, Mg)Ni$_3$	12.27	5.051	24.316	537.15
	(La, Mg)$_2$Ni$_7$	60.28	5.057	24.442	541.32
0.4	LaNi$_5$	38.53	5.051	4.037	89.20
	(La, Mg)Ni$_3$	13.69	5.048	24.390	538.23
	(La, Mg)$_2$Ni$_7$	47.78	5.064	24.497	544.04
0.5	LaNi$_5$	46.76	5.062	4.046	89.78
	(La, Mg)Ni$_3$	15.26	5.052	24.435	540.02
	(La, Mg)$_2$Ni$_7$	37.98	5.071	24.505	545.72

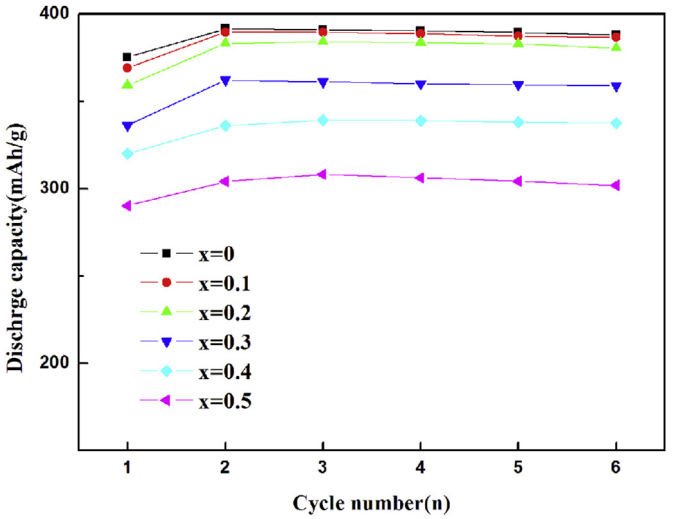

Fig. 4. Activation curves of $La_{0.6}Gd_{0.2}Mg_{0.2}Ni_{3.0}Co_{0.5-x}Al_x$ ($x = 0$–0.5) alloy electrodes at 298 K.

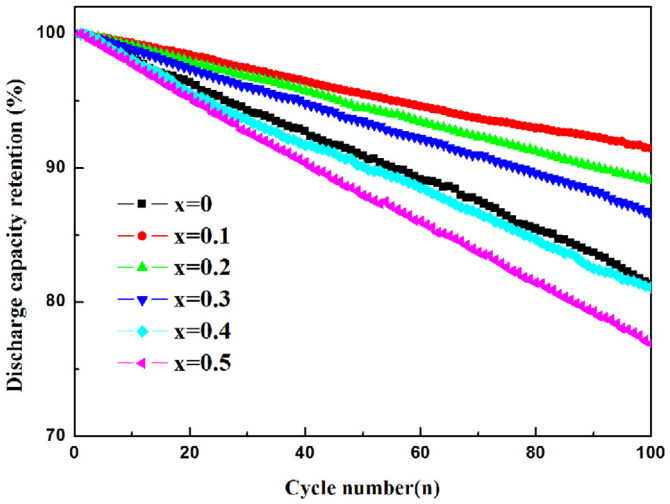

Fig. 5. Cyclic stability curves of $La_{0.6}Gd_{0.2}Mg_{0.2}Ni_{3.0}Co_{0.5-x}Al_x$ ($x = 0$–0.5) alloy electrodes at 298 K.

illustrates the cyclic stability curves of $La_{0.6}Gd_{0.2}Mg_{0.2}Ni_{3.0}Co_{0.5-x}Al_x$ ($x = 0$–0.5) alloy electrodes. The figure reveals that the discharge capacity retention of all alloy electrodes decays gradually with cycle number increasing. Moreover, it can be seen that the curves of the alloy electrodes with $0.1 \leq x \leq 0.3$ become flatter than that of the other curves, which indicates the cyclic stability of these alloy electrodes were noticeably improved. From Table 2, it is known that after 100 charge/discharge cycles, the discharge capacity retention of the alloy electrodes increases from 81.3% ($x = 0$) to 91.5% ($x = 0.1$) firstly, and then decreases to 76.9% ($x = 0.5$).

It is well known that the discharge capacity degradation of metal-hydride electrodes can be influenced primarily by two factors, the surface passivation due to the formation of surface oxide/hydroxide and pulverization of alloy particles owing to cell volume expansion during hydrogen absorption/desorption process [16,17]. Fig. 6 shows SEM images of $La_{0.6}Gd_{0.2}Mg_{0.2}Ni_{3.0}Co_{0.5-x}Al_x$ ($x = 0$, 0.1, 0.3, 0.5) alloy electrodes before and after different cycles. It is evident that all alloy particles possess the same status without charge/discharge cycles. After 10 cycles, for the samples of $x = 0$, $x = 0.1$ and $x = 0.3$, there are only a few fine cracks appeared on the alloy surface while the sample of $x = 0.5$ displays more cracks. After 20 cycles, the cracks condition of $x = 0.1$ is still not change a lot. However, the samples of $x = 0$ and $x = 0.3$ show more and deeper cracks than themselves after 10 cycles. The sample of $x = 0.5$ reveals a large amount of cracks and the alloy has been crumbled into many small particles. Based on the microstructure analyses, the unit cell volumes of various phases increase linearly with increasing Al content which reduce the volume expansion/contraction during the charge/discharge cycles of the alloy electrodes and lower the pulverization process of alloy electrodes. As a result, the alloy electrode with $x = 0.1$ reveals better anti-pulverization capability than the alloy without Al substitution. However, $(La, Mg)_2Ni_7$ phase, $LaNi_5$ phase and $(La, Mg)\ Ni_3$ phase exhibit different cell volume expansions during the charge/discharge cycles [18]. As Al content increasing further ($x > 0.1$), more and more $(La, Mg)_2Ni_7$ phase transforms to $LaNi_5$ phase and $(La, Mg)\ Ni_3$ phase which increases the discrete volume expansion among different phases and accelerates the pulverization rate of the alloys during cycles. The results about the differences of crack condition between alloy particles and the analyses for discharge capacity retention confirm that the proper Al substitution for Co ($0.1 \leq x \leq 0.3$) can slow down the pulverization process and improve the cyclic stability of the alloy electrodes.

Table 2
Electrochemical characteristics of $La_{0.6}Gd_{0.2}Mg_{0.2}Ni_{3.0}Co_{0.5-x}Al_x$ ($x = 0$–0.5) alloy electrodes.

Sample	Na[a]	C_{max} (mAh/g)	S_{100} (%)	i_{corr} (mA cm^{-2})
$x = 0.0$	2	391.5	81.3	16.5
$x = 0.1$	2	389.8	91.5	8.9
$x = 0.2$	3	384.3	89.1	10.1
$x = 0.3$	3	362.3	86.5	12.1
$x = 0.4$	3	339.4	81.1	16.8
$x = 0.5$	3	308.4	76.9	17.9

[a] The cycle numbers needed to activate the electrodes.

It is come to light that the oxidation/corrosion rates of the alloy electrodes in the alkaline electrolyte can be characterized by the corrosion current density i_{corr} which can be determined by the Tafel extrapolation method [19]. Fig. 7 shows the Tafel polarization curves of $La_{0.6}Gd_{0.2}Mg_{0.2}Ni_{3.0}Co_{0.5-x}Al_x$ ($x = 0$–0.5) alloy electrodes and the corrosion current density i_{corr} can be obtained and listed in Table 2. It can be seen that the order of i_{corr} is: $x = 0.5 > x = 0$ and $x = 0.4 > x = 0.3 > x = 0.2 > x = 0.1$. The results about the i_{corr} reveal that the anti-oxidation capability order of the alloy electrodes is: $x = 0.1 > x = 0.2 > x = 0.3 > x = 0$ and $x = 0.4 > x = 0.5$ which is in accordance with the variation of cyclic stability of the alloy electrodes. Synthesize discharge capacity and cyclic stability, the alloy electrode with $x = 0.1$ possesses better electrochemical properties than others.

3.4. High rate dischargeability

The high rate dischargeability reflects the electrochemical hydrogen storage kinetics of the alloy electrodes which has been regarded as an important factor for Ni/MH batteries. Fig. 8 shows the effect of discharge current density (300–900 mA g^{-1}) on the high rate dischargeability (HRD) of $La_{0.6}Gd_{0.2}Mg_{0.2}Ni_{3.0}Co_{0.5-x}Al_x$ ($x = 0$–0.5) alloy electrodes. It can be seen that the HRDs of the alloy electrodes are almost unchanged when $x \leq 0.1$, and then decrease when $x \geq 0.2$. Table 3 lists the HRDs of the alloy electrodes at discharge current density of 900 mA g^{-1}. From Table 3, it can be found that the HRD_{900} decreases from 79.3% ($x = 0$) to 78.4% ($x = 0.1$) slightly, and then decreases gradually to 60.5% ($x = 0.5$).

It is known that the HRD characteristic stands for overall kinetic properties and is influenced mainly by charge transfer on surface of alloy electrodes and hydrogen diffusion in alloy bulk [20]. To

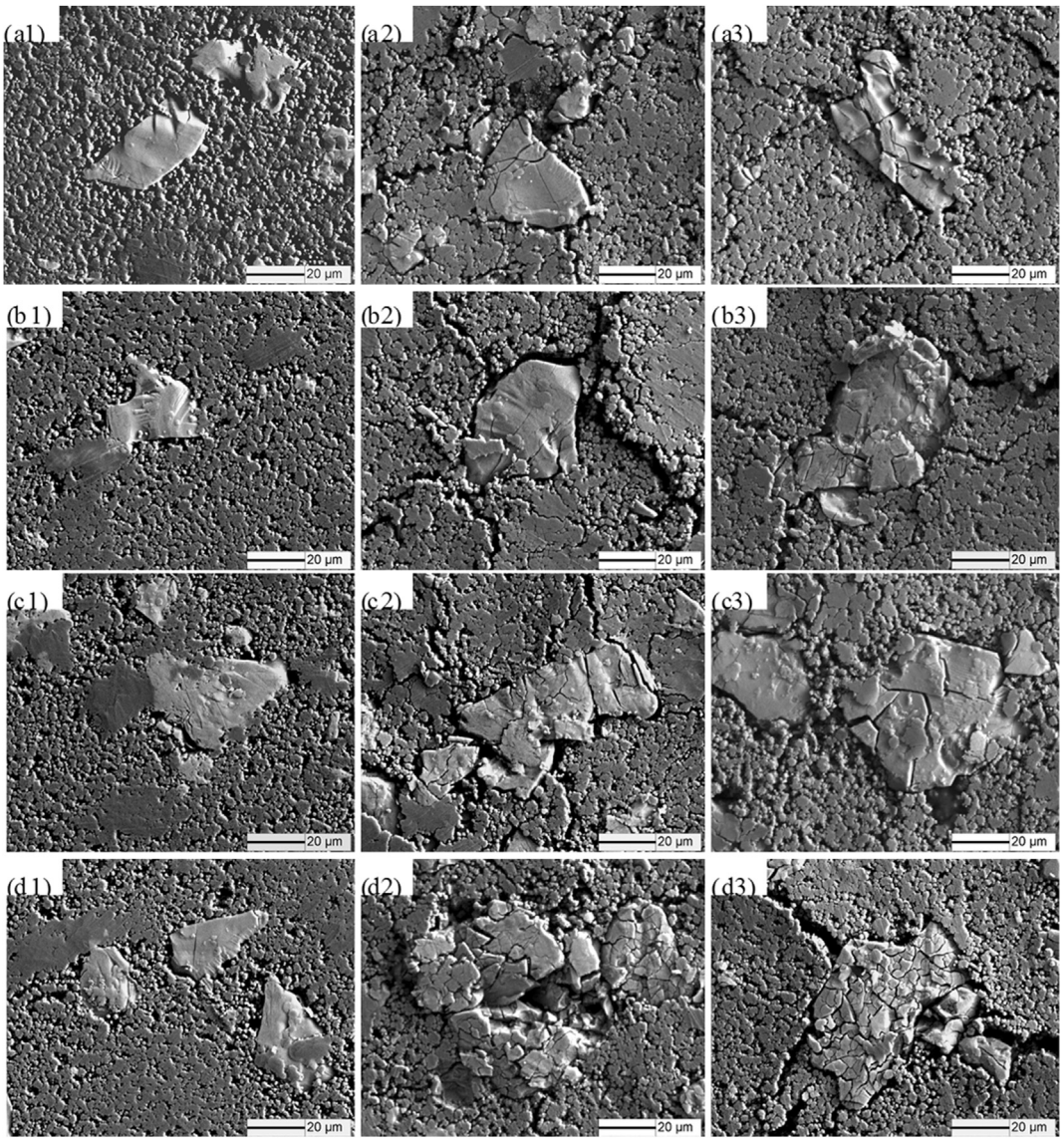

Fig. 6. SEM images of $La_{0.6}Gd_{0.2}Mg_{0.2}Ni_{3.0}Co_{0.5-x}Al_x$ (x = 0, 0.1, 0.3, 0.5) alloy electrodes before and after cycling: (a1, b1, c1, d1) x = 0, 0.1, 0.3, 0.5 alloy electrodes before cycling respectively; (a2, b2, c2, d2) x = 0, 0.1, 0.3, 0.5 alloy electrodes after 10 cycles respectively; (a3, b3, c3, d3) x = 0, 0.1, 0.3, 0.5 alloy electrodes after 20 cycles respectively.

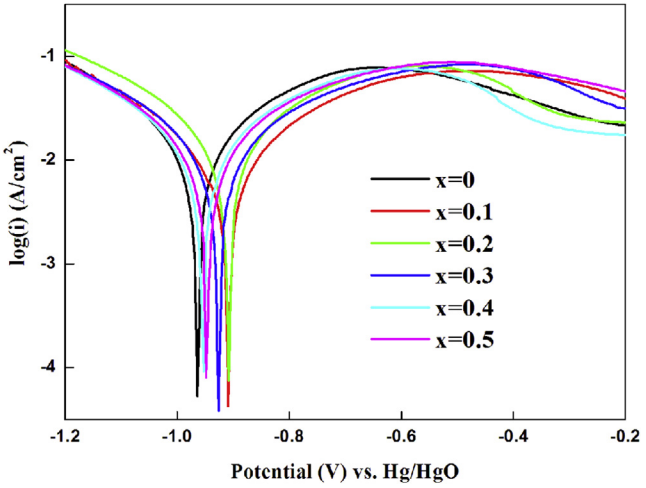

Fig. 7. Tafel polarization curves of $La_{0.6}Gd_{0.2}Mg_{0.2}Ni_{3.0}Co_{0.5-x}Al_x$ (x = 0–0.5) alloy electrodes at 50% DOD and 298 K.

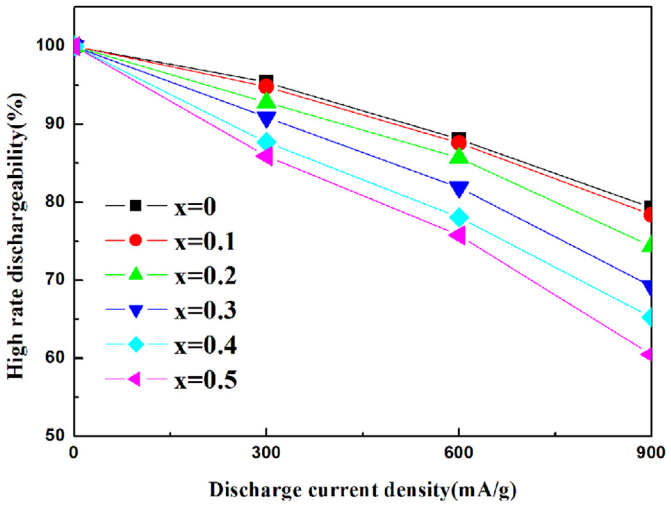

Fig. 8. High rate dischargeability (HRD) of $La_{0.6}Gd_{0.2}Mg_{0.2}Ni_{3.0}Co_{0.5-x}Al_x$ (x = 0–0.5) alloy electrodes at 298 K.

Table 3
Electrochemical kinetic parameters of $La_{0.6}Gd_{0.2}Mg_{0.2}Ni_{3.0}Co_{0.5-x}Al_x$ ($x = 0$–0.5) alloy electrodes.

Sample	HRD_{900} (%)	I_0 (mA g^{-1})	D_0 (cm^2 s^{-1})
$x = 0$	79.3	309.1	3.3×10^{-10}
$x = 0.1$	78.4	305.4	3.5×10^{-10}
$x = 0.2$	74.4	289.9	4.1×10^{-10}
$x = 0.3$	69.2	277.2	4.4×10^{-10}
$x = 0.4$	65.3	267.7	4.9×10^{-10}
$x = 0.5$	60.5	259.2	5.7×10^{-10}

investigate the effect of the partial substitution of Al for Co on the discharge kinetics, linear polarization, potential-step discharge experiment were performed on these alloy electrodes. Table 3 summarized the kinetic characteristics of $La_{0.6}Gd_{0.2}Mg_{0.2}Ni_{3.0-Co_{0.5-x}Al_x}$ ($x = 0$–0.5) alloy electrodes. Exchange current density I_0, as an important kinetic parameter, is used to evaluate the speed of charge transfer on surface of alloy electrodes and can be calculated according to the following equation [21]:

$$I_0 = \frac{RTI_d}{F\eta} \tag{2}$$

where R is the gas constant, T is the absolute temperature, F is the Faraday constant, I_d is the applied current density and η is the overpotential. Fig. 9 shows the linear polarization curves of the alloy electrodes at 50% DOD and 298 K. As shown in Fig. 9 and Table 3, I_0 decreases from 309.1 mA g^{-1} ($x = 0$) to 259.2 mA g^{-1} ($x = 0.5$). After Al substitution for Co, Al oxide films formed on alloy surfaces and the content of oxide gradually increases with increasing Al content. The increasing oxide content on alloy surfaces leads to the increase of the charge transfer resistance and lower the exchange current density I_0.

Besides I_0, the hydrogen diffusion coefficient D_0 is the other important kinetic parameter which is used to describe the hydrogen diffusivity in the bulk of the alloys and can be attained according to the following equation [22]:

$$\log i = \left(\frac{6FD(C_0 - C_s)}{da^2}\right) - \frac{\pi^2}{2.303}\frac{D_0}{a^2}t \tag{3}$$

where i, D_0, C_0, C_s, d, a and t are the diffusion current density (A g^{-1}), the hydrogen diffusion coefficient (cm^2 s^{-1}), the initial hydrogen concentration in the bulk of the alloy (mol cm^{-3}), the hydrogen concentration on the surface of the alloy particles (mol cm^{-3}), the density of the hydrogen storage alloy (g cm^{-3}), the alloy particle radius (cm) and the discharge time(s), respectively. Fig. 10 represents the semilogarithmic curves of anodic current-discharge time response of $La_{0.6}Gd_{0.2}Mg_{0.2}Ni_{3.0}Co_{0.5-x}Al_x$ ($x = 0$–0.5) alloys electrodes at fully charged state and 298 K. D_0 value can be estimated according to the slop of log(i) versus t by Equation (3) and are listed in Table 3. It can be seen that the hydrogen diffusion coefficient D_0 increases with the Al content increasing and reaches the maximum when $x = 0.5$. It is found that the presence of multiphase interfaces can provide channels for hydrogen diffusion and increase the hydrogen atoms desorbing from the hydride reaction [23]. It is known that the abundance of $LaNi_5$ phase and (La, Mg)Ni_3 phase increases with Al content increasing which can provide larger area of interface. The increasing area of interface leads to the improvement of hydrogen diffusion for $La_{0.6}Gd_{0.2}Mg_{0.2}Ni_{3.0}Co_{0.5-x}Al_x$ ($x = 0$–0.5) alloy electrodes. Combining exchange current density I_0 and the hydrogen diffusion coefficient D_0, it can be observed that the variation of I_0 is in good agreement with that of the HRD_{900}, which indicates that the charge transfer on alloy surface is more important for the electrochemical kinetic properties of alloy electrodes.

4. Conclusions

In this paper, the crystal structure and electrochemical performance of $La_{0.6}Gd_{0.2}Mg_{0.2}Ni_{3.0}Co_{0.5-x}Al_x$ ($x = 0$–0.5) hydrogen storage alloys have been studied systematically. Some conclusions can be summarized as follows:

1. All alloys are composed of $(La, Mg)_2Ni_7$ phase, (La, Mg)Ni_3 phase and $LaNi_5$ phase. As Al content increasing, the $(La, Mg)_2Ni_7$ phase were decomposed into (La, Mg)Ni_3 and $LaNi_5$ phase and the abundance of $(La, Mg)_2Ni_7$ phase decreases from 91.09% ($x = 0$) to 37.98% ($x = 0.5$) while the abundance of (La, Mg)Ni_3 and $LaNi_5$ phase increase linearly.
2. All alloy electrodes exhibit the perfect activation properties and the maximum discharge capacity of the alloy electrodes decreases with increasing Al content. The cyclic stability of alloy

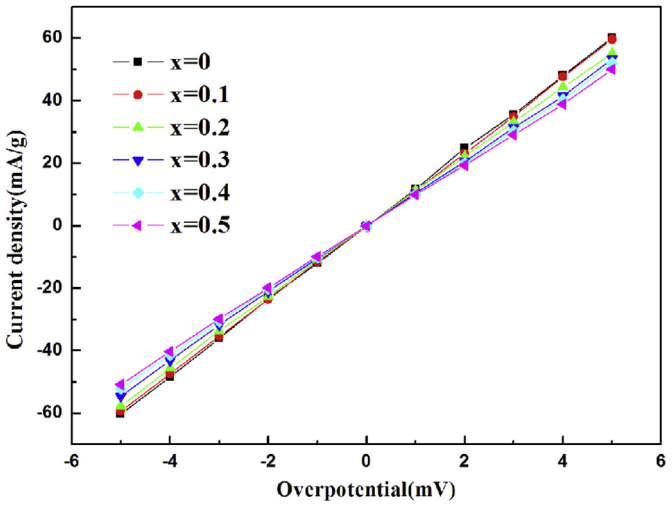

Fig. 9. Linear polarization curves of $La_{0.6}Gd_{0.2}Mg_{0.2}Ni_{3.0}Co_{0.5-x}Al_x$ ($x = 0$–0.5) alloy electrodes at 50% DOD and 298 K.

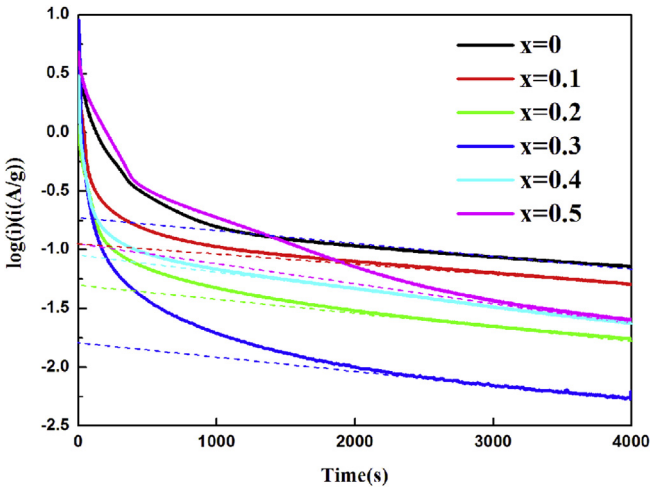

Fig. 10. Semilogarithmic curves of anodic current–discharge time response of $La_{0.6}Gd_{0.2}Mg_{0.2}Ni_{3.0}Co_{0.5-x}Al_x$ ($x = 0$–0.5) alloys electrodes at fully charged state and 298 K.

electrodes are improved from 81.3% ($x = 0$) to 91.5% ($x = 0.1$) which is attributed to the lower pulverization rate and the better anti-corrosion capability of the alloy electrodes after proper Al substitution for Co.

3. The HRDs of the alloy electrodes decrease with Al content increasing. The HRDs analyses reveal that the charge transfer on alloy surface is more important than the hydrogen diffusion in alloy bulk for the kinetic properties of the alloy electrodes.

Acknowledgments

This work was supported by the National High-Tech Research and Development Program of China (Grant No. 2011AA03A408), the National Basic Research Program of China (Grant No. 2011GB111003) and the National Natural Science Foundation of China (Grant No. 51102006).

References

[1] Y.H. Zhang, Y. Cai, C. Zhao, T.T. Zhai, G.F. Zhang, D.L. Zhao, Int. J. Hydrogen Energy 37 (2012) 14590–14597.
[2] Y.H. Zhang, Z.G. Hou, B.W. Li, H.P. Ren, F.Z. Zhang, D.L. Zhao, J. Alloys Compd. 537 (2012) 175–182.
[3] Y. Li, S.M. Han, Z.P. Liu, Int. J. Hydrogen Energy 35 (2010) 12858–12863.
[4] H. Miao, H.G. Pan, S.C. Zhang, N. Chen, R. Li, M.X. Gao, Int. J. Hydrogen Energy 32 (2007) 3387–3394.
[5] B. Liao, Y.Q. Lei, L.X. Chen, G.L. Lu, H.G. Pan, Q.D. Wang, Electrochim. Acta 50 (2004) 1057–1063.
[6] P.H.L. Notten, P. Hokkeling, J. Electrochim. Soc. 138 (1991) 1877–1885.
[7] Y.F. Liu, H.G. Pan, Y.J. Yue, X.F. Wu, N. Chen, Y.Q. Lei, J. Alloys Compd. 395 (2005) 291–299.
[8] X.B. Zhang, D.Z. Sun, W.Y. Yin, Y.J. Chai, M.S. Zhao, Electrochim. Acta 50 (2005) 3407–3413.
[9] Y.F. Liu, H.G. Pan, M.X. Gao, H. Miao, Y.Q. Lei, Q.D. Wang, Int. J. Hydrogen Energy 33 (2008) 124–133.
[10] B. Liao, Y.Q. Lei, L.X. Chen, G.L. Lu, H.G. Pan, Q.D. Wang, J. Alloys Compd. 404 (2005) 665–668.
[11] J. Guo, R. Zhang, W.Q. Jiang, G.X. Li, W.L. Wei, J. Alloys Compd. 429 (2007) 348–351.
[12] B. Liao, Y.Q. Lei, L.X. Chen, G.L. Lu, H.G. Pan, Q.D. Wang, J. Alloys Compd. 376 (2004) 186–195.
[13] Z.J. Gao, Y.C. Luo, R.F. Li, Z. Lin, L. Kang, J. Power Sources 241 (2013) 509–516.
[14] Y.H. Zhang, G.Q. Wang, X.P. Dong, S.H. Guo, J.M. Wu, X.L. Wang, J. Alloys Compd. 379 (2004) 298–304.
[15] T. Ozaki, M. Kanemoto, T. Kakeya, Y. Kitano, M. Kuzuhara, M. Watada, S. Tanase, T. Sakai, J. Alloys Compd. 446–447 (2007) 620–624.
[16] J.J.G. Willems, K.H.J. Buschow, J. Less-Common Met. 129 (1987) 13–30.
[17] M.B. Moussaa, M. Abdellaoui, C. Khaldi, H. Mathlouthi, J. Lamloumi, A.G. Percheron, J. Alloys Compd. 399 (2005) 264–269.
[18] J.J. Liu, S.M. Han, Y. Li, S.Q. Yang, W.Z. Shen, L. Zhang, Y. Zhou, J. Alloys Compd. 552 (2013) 119–126.
[19] E. McCafferty, Corros. Sci. 47 (2005) 3202–3215.
[20] C. Iwakura, M. Matsuoka, K. Asai, T. Kohno, J. Power Sources 38 (1992) 335–343.
[21] X.Q. Shen, Y.G. Chen, M.D. Tao, C.L. Wu, G. Deng, Z.Z. Kang, Int. J. Hydrogen Energy 34 (2009) 2661–2669.
[22] G. Zheng, B.N. Popov, R.E. White, J. Electrochem Soc. 142 (1) (1995) 154–156.
[23] R. Tang, L.Q. Liu, Y.N. Liu, G. Yu, Int. J. Hydrogen Energy 28 (2003) 815–819.